**Astronomy
&
Astrophysics**

Dust properties of protoplanetary disks in the Taurus-Auriga star forming region from millimeter wavelengths

L. Ricci[1], L. Testi[1,2], A. Natta[2], R. Neri[3], S. Cabrit[4], and G. J. Herczeg[5]

[1] European Southern Observatory, Karl-Schwarzschild-Strasse 2, 85748 Garching, Germany
 e-mail: lricci@eso.org
[2] INAF - Osservatorio Astrofisico di Arcetri, Largo Fermi 5, 50125 Firenze, Italy
[3] Institut de Radioastronomie Millimétrique, 300 rue de la Piscine, 38406 Saint Martin d'Hères, France
[4] LERMA, UMR 8112 du CNRS, Observatoire de Paris, 61 Av. de l'Observatoire, 75014 Paris, France
[5] Max Planck Institut fur Extraterrestrische Physik, Postfach 1312, 85741 Garching, Germany

ABSTRACT

We present the most sensitive 3 mm-survey to date of protoplanetary disks carried out in the Taurus-Auriga star forming region (average rms of about 0.3 mJy), using the IRAM PdBI. With our high detection rate of 17/19 we provide the first detections at wavelengths longer than about 1 mm for 12 sources. This enables us to statistically study the mm SED slopes and dust properties of faint disks and compare them to brighter disks using a uniform analysis method. With these new data and literature measurements at sub-millimeter and millimeter wavelengths, we analyze the dust properties of a sample of 21 isolated disks around T Tauri stars in the Taurus-Auriga star forming region. Together with the information about the disks' spatial extension from sub/mm-mm interferometric studies, we derive from the observed sub-mm/mm spectral energy distribution constraints on the dust opacity law at these wavelengths, using two-layer flared disk models and a self-consistent dust model that properly takes into account the variation of the dust opacity with grain growth. We find evidence for the presence of dust particles in the disk midplane that have grown to sizes as large as at least 1 millimeter in all the disks of our sample, confirming what was previously observed on smaller brighter objects. This indicates that the dust coagulation from ISM dust to mm-sized grains is a very fast process in protoplanetary disks, which appears to occur before a young stellar object enters the class II evolutionary stage. The amount of these large grains in the disk outer regions is also found to be stationary throughout the whole class II evolutionary stage, which indicates that mechanisms slowing down the dust inward migration play an important role in the Taurus-Auriga protoplanetary disks. Another result is that the spectral index between 1 and 3 mm for the six faintest disks in our sample is on average smaller than for the brighter disks, indicating either that these fainter yet unmapped disks are spatially much less extended than the brighter spatially resolved disks, or that fainter disks have typically larger dust grains in their outer regions. Considering that these fainter disks are more representative of the bulk of the disk population than the brighter ones, this may have important consequences for the theories of planetesimal formation and disk formation and evolution. Finally, we investigate the relations between the derived dust properties, namely dust mass and grain growth, and the properties of the central star, like its mass, age and mass accretion rate.

Key words. protoplanetary disks – stars: pre-main sequence – planets and satellites: formation

1. Introduction

Circumstellar disks play a fundamental role in the physical processes involved in star and planet formation. In these systems part of the material (gas and dust) loses its angular momentum and accretes onto the central forming star, while another part of it may give birth to a planetary system. Although the content of dust is only a small fraction of the overall material in a circumstellar disk, dust grains are crucial elements in the early stages of planet formation. According to the core-accretion scenario (Safronov & Zvjagina 1969; Pollack et al. 1996), growth from an initial ISM population of submicrometer-sized dust grains to planetesimals of $1-100$ km sizes is believed to be the key mechanism of early planet formation. These planetesimal "embryos" then continue to grow which leads to the formation of at least terrestrial-sized planets and possibly the cores of giant planets.

Observational evidence of grain growth from the ISM dust has been obtained from a variety of techniques at different wavelengths. Throop et al. (2001) observed in the optical and near-infrared the translucent edge of the 114–426 protoplanetary disk in the Orion Nebula Cluster, and derived from the extinction curve of the background nebular emission a lower limit of a few microns for the dust grains in the far outer regions of the disk, about 500 AU away from the central star. Another method to probe the presence of large grains in the disk is through the shape and intensity of the 10- and 20-μm silicate features. The data indicate a broad variety of silicate profiles, ranging from strongly peaked silicate bands and steeply rising spectral energy distributions (SEDs) to "boxy" silicate profiles and flatter SEDs (ISO, Malfait et al. 1998; Spitzer Space Telescope, Kessler-Silacci et al. 2006). The boxy features with low feature-to-continuum ratios are interpreted as grain growth to micron size (Bouwman et al. 2001).

However, the techniques outlined so far can only probe dust grains as large as some μm in the disk surface layers. They are not sensitive to larger grains in the disk midplane, the region in which planet formation is supposed to occur. In order to probe larger grains in the midplane, observations at millimeter wavelengths are needed. Beckwith & Sargent (1991) showed that T Tauri stars have shallow SEDs at sub-millimeter wavelengths.

Under the assumption of optically thin emission at these frequencies, this implies a dust opacity dependence on wavelength ($\kappa_{mm} \propto \lambda^{-\beta}$) much flatter than in the ISM ($\beta_{ISM} = 1.7$), which is naturally interpreted in terms of grain growth (see e.g. Draine 2006). However, this interpretation of the disk SEDs is not unique, since the same data can be explained by very small optically thick disks. To break this degeneracy and sort out the effect of a potentially large optical depth it is necessary to spatially resolve the disks to determine their actual sizes. Furthermore, in this context observations at millimeter wavelengths are very useful, since at these lower frequencies the impact of optically thick disk inner regions to the total emission is expected to be lower. Therefore, to actually probe the dust properties in protoplanetary disks, one needs to combine the determination of the sub-millimeter/millimeter SED with information on the disk extension from high-angular resolution interferometric observations (see e.g. Testi et al. 2001).

In the last years, several sub-mm/mm interferometric observations have been carried out to investigate dust grain growth in protoplanetary disks. Wilner et al. (2000) resolved the disk around the TW Hya pre-main-sequence (PMS) star at 7 mm using the Very Large Array (VLA). Extensive modeling of the SED of this source has shown that the dust grains in the outer parts of the TW Hya disk have grown to at least ~1 cm (Calvet et al. 2002). An analogous result has been obtained for the disk around CQ Tau (Testi et al. 2003). More recently, Rodmann et al. (2006) resolved ten disks in the Taurus-Auriga star forming region and found clear evidence of grain growth in four of them. Lommen et al. (2007) resolved one disk in Chamaeleon and four in Lupus with the Submillimeter Array (SMA) at 1.4 mm and with the Australia Telescope Compact Array (ATCA) at 3.3 mm, and found clear evidence of dust grain growth to sizes of a few millimeters for four of them. Finally Schaefer et al. (2009) observed a sample of 23 low mass PMS stars (with spectral types of K7 and later) in Taurus-Auriga at 1.3 mm and 2.6 mm with the Plateau de Bure Interferometer (PdBI); they detected only eight sources at 1.3 mm and six at 2.6 mm, and found evidence of grain growth for the three disks that they could spatially resolve.

In this paper we present our analysis on 21 protoplanetary disks around T Tauri stars in the Taurus-Auriga star forming region without stellar companions in the range of 0.05″–3.5″. For eleven of these objects, mainly faint disks with $F_{1.3\ mm} < 100$ mJy, we have obtained new data at ~3 mm with the Plateau de Bure Interferometer[1] (hereafter PdBI) with an average rms of about 0.3 mJy. Together with the data already present in the literature at sub/mm- and mm-wavelengths, and with the information obtained in the last years on the disks' spatial extension from high-angular resolution interferometric observations at mm wavelengths, we investigate the dust properties in the disks, namely grain growth and dust mass, and their relation with the properties of the central star.

In Sect. 2 we present our new PdBI data, the properties of our sample, the method we used to estimate the main stellar physical quantities, and the data we used for our analysis. In Sect. 3 we describe the disk models adopted for the analysis of the disks sub-mm/mm SED. In Sect. 4 we show and discuss the results of our study in terms of dust grain growth and dust mass, whereas in Sect. 5 we summarize our main findings.

---

2. New 3 mm observations and sample properties

2.1. New PdBI observations

We observed a total list of 19 targets; 16 of them were selected to be relatively faint, with 15 mJy $<F_{1.3mm}<$ 100 mJy and with no known detections beyond about 1 mm; the other three (HL, DO and DR Tau) are brighter sources that were observed for reference purposes. The observations were carried out with PdBI between July and August 2007. Owing to antenna maintenance work, all observations were carried out in a subarray of the six-element interferometer. The antennae were arranged in very compact configurations that provided sensitive baselines from 15 m to 80 m. The dual-polarization receivers, which were observing in the 3 mm band, had typical receiver temperatures of about 35 K and were providing image sideband rejection values better than 10 dB. To achieve maximum sensitivity in the continuum, the spectral correlator was adjusted to cover a total effective bandwidth of about 2 GHz.

The observing procedures were set up to fill in gaps in the scheduling without any specific tuning wavelength within the 3 mm band. Visibilities were obtained using on-source integration times of 22 min interspersed with 2 min calibrations on a nearby calibrator. Each star was observed on one or more occasions for a minimum of 40 min and a maximum of 2 h on-source. The atmospheric phase stability on the baselines was always better than 40°, consistent with seeing conditions of 1″–3″, typical for summer. The absolute flux density scale was calibrated on 3C84, 0528+134, MWC349 and Mars, and was found to be accurate to 10%. The receiver passband shape was determined with excellent precision on a strong calibrator like 3C84.

We used the GILDAS package for the data reduction and analysis. The data were calibrated in the antenna based manner. The continuum visibilities were gridded with natural weighting and no taper to maximize the sensitivity. Since none of the target stars was found to be resolved in synthesized beams of 2″–4″, a point source model was fitted to the calibrated visibilities of each star to estimate the flux density of the continuum in the 3 mm band. The results are summarized in Table 1. Among the 19 targets, 17 were detected, including 14 of the 16 faint sources, thanks to our good sensitivity; 12 of these are first detections longward of about 1 mm, which strongly expands the available database of 3 mm data towards fainter disks. The 2.6 mm detections of LkHa 358 and GO Tau were recently published by Schaefer et al. (2009).

In Sects. 2.2, 2.3 and 2.4 we describe the final sample used for our analysis of dust properties, the adopted method to estimate the stellar properties and mass accretion rates summarized in Table 2, whereas in Sect. 2.5 we report the sub-mm/mm data that we collected from the literature for our analysis.

2.2. Sample

Our final sample of 21 sources consists of all young stellar objects (YSO) in Taurus-Auriga catalogued in Andrews & Williams (2005) which fulfil the following criteria: (1) a class II infrared SED, to avoid contamination of sub-mm fluxes by a residual envelope; (2) information on the central star through optical-NIR spectroscopic/photometric data, necessary to calculate self-consistent disk SED models; (3) one detection at ~3 mm (either from our new PdBI observations or from the literature) and at least one detection in the 0.45 mm < λ < 0.85 mm spectral region. This selection criterion was chosen to probe a broad enough spectral window to efficiently constrain the

Table 1. Summary of the new PdBI observations.

Object	α (J2000)	δ (J2000)	ν (GHz)	λ (mm)	F_ν (mJy)	rms (mJy)	Comments[1]
CW Tau	04:14:17.0	28:10:56.51	84.2	3.57	3.44	0.31	
CX Tau	04:14:47.8	26:48:11.16	86.2	3.49	1.01	0.13	
DE Tau	04:21:55.6	27:55:05.55	92.6	3.23	3.32	0.25	
DK Tau	04:30:44.3	26:01:23.96	84.2	3.57	4.70	0.20	2.5″ binary
DO Tau	04:38:28.6	26:10:49.76	84.2	3.57	13.80	0.29	
DP Tau	04:42:37.7	25:15:37.56	84.2	3.57	<0.78	0.26	no sub-mm info
DR Tau	04:47:06.2	16:58:43.05	100.8	2.97	13.90	0.47	
DS Tau	04:47:48.6	29:25:10.96	100.8	2.97	2.96	0.21	
FM Tau	04:14:13.5	28:12:48.84	100.8	2.97	2.65	0.24	
FP Tau	04:14:47.4	26:46:26.65	100.8	2.97	11.80	0.26	no sub-mm info
FY Tau	04:32:30.5	24:19:56.69	100.8	2.97	1.90	0.28	no sub-mm info
FZ Tau	04:32:31.8	24:20:02.53	100.8	2.97	2.89	0.24	
GK Tau	04:33:34.6	24:21:06.07	100.8	2.97	<0.96	0.32	2.5″ binary
GO Tau	04:43:03.1	25:20:17.38	86.2	3.49	4.05	0.34	
Haro 6-28	04:35:56.9	22:54:36.63	87.0	3.45	0.92	0.18	0.7″ binary
HL Tau	04:31:38.4	18:13:57.37	84.5	3.53	43.40	0.68	flat spectrum
HO Tau	04:35:20.2	22:32:13.98	87.0	3.45	2.03	0.53	
LkHa 358	04:31:36.2	18:13:43.20	84.5	3.53	2.46	0.22	no sub-mm info
SU Aur	04:55:59.4	30:34:10.39	84.5	3.53	2.88	0.19	

Notes. [1] Reason why the source has not been considered in the analysis (see text for more details).

optically thin part of the sub-mm/mm spectral energy distribution (SED); (4) no evidence of stellar companions in the 0.05−3.5″ range in angular separation. This range corresponds to about 5−500 AU in projected physical separation at the Taurus-Auriga star forming region distance, here assumed to be 140 pc for all the sources of our sample (Bertout et al. 1999). The limit of 3.5 arcsec ensures that mm interferometric flux measurements, of a typical resolution of 1 arcsec, are not contaminated by the companion's disk, while binaries closer than 5 AU should have outer disk properties similar to those of single stars on the scales probed by (sub-)mm data.

Only 21 sources catalogued by Andrews & Williams (2005) fulfil the above four criteria. They are listed in Table 2 and include eleven sources from our PdBI sample[2].

Figure 1 reports histograms that describe the completeness level of our final sample with respect to all Taurus-Auriga class II YSOs catalogued in Andrews & Williams (2005), and fulfilling the "isolation" criterion (4). Our sample contains 63% of these "isolated" class II showing a flux at ~0.85 mm greater than 100 mJy, and 31% of the sources with lower 0.85 mm fluxes. Therefore our sample is not complete even for the brightest YSOs at 0.85 mm. This is due to a lack of observations at ~3 mm for these sources. However, thanks to the high sensitivity of our new PdBI observations (see Sect. 2.1) our sample enables us to study statistically the dust properties of faint disks

(i.e. with $F_{1.3\,mm}$ < 100 mJy, $F_{0.85\,mm}$ < 100 mJy) for the first time and compare them to the brighter ones using a uniform analysis method. In terms of the stellar properties, it is important to note that the Andrews & Williams (2005) catalogue includes only a few very low mass PMS stars: only stars with an estimated mass higher than about 0.2 $M_\odot$ have been detected because of the sensitivity limits of the current facilities at sub-mm and mm wavelengths that make the detection of disks around very low mass YSOs very difficult. The sensitivity limitation is even more severe at 3 mm, therefore our final sample includes 58% of all the class II isolated sample of Andrews & Williams (2005) with an estimated mass greater than 0.4 $M_\odot$, but only two sources with $M_\star$ < 0.4 $M_\odot$ (out of ten in Andrews & Williams 2005).

2.3. Stellar properties

Spectral types for all the sources in our sample are taken from the literature (Kenyon & Hartmann 1995, Briceño et al. 1998) and cover a range from G2 (SU Aur) to M2.5 (CX Tau). Spectral types of M0 and earlier have been converted to effective temperatures with the dwarf temperature scale of Schmidt-Kaler (1982), whereas for types later than M0 we adopted the temperature scale developed by Luhman 1999. Typical uncertainties for these sources are ~1–1.5 in spectral sub-types or ~100–150 K in temperature.

The stellar luminosities of all the pre-main-sequence (PMS) stars were computed from their J-band flux (2MASS All Sky Catalog of point sources, Cutri et al. 2003) to minimize contamination from UV and IR excess emission. For the bolometric corrections we adopted the dwarf values from Kenyon & Hartmann (1995) that are considered to be satisfactory approximations for these young sources in the J-band (Luhman 1999).

In order to estimate the amount of extinction toward these young sources, we calculated the color excesses using intrinsic colors provided by Kenyon & Hartmann (1995) for the G2−K7 spectral types and by Leggett (1992) for the M0−M2.5 types. To ensure that the color excess reflects only the effect of reddening,

---

[2] The eight sources dropped from the PdBI sample are HL Tau (a flat spectrum source that retains an envelope; Padgett et al. 1999); DP Tau, FP Tau, FY Tau and LkHa 358 that have no available submm detections for SED fitting; and DK Tau, GK Tau and Haro 6−28 which are binary systems with angular separations of 2.5″ (Simon et al. 1992), 2.5″ (Reipurth & Zinnecker 1993) and 0.7″ (Leinert et al. 1993) respectively. We keep in our sample the wide binaries DS Tau and HO Tau (angular separations of 7.1″ and 6.9″ respectively, Mathieu et al. 1994); they do not show any emission from the companions from our new 3 mm interferometric observations. The other dropped multiple systems from the AW05 catalog are DH Tau (2.3″ binary, Itoh et al. 2005), GG Tau (quadruple system with a circumbinary ring of inner and outer radii of 180 and 260 AU respectively, Pinte et al. 2007), and UY Aur (0.9″ binary, Leinert et al. 1993).

Table 2. Stellar properties.

Object	ST	$T_{\rm eff}$ (K)	$L_\star$ ($L_\odot$)	$L_{\rm acc}$ ($L_\odot$)	Ref. ($L_{\rm acc}$)	$R_\star$ ($R_\odot$)	Log $\dot{M}_{\rm acc}$ ($M_\odot$ yr^{-1})	$M_\star$ ($M_\odot$)	Age (Myr)
AA Tau	K7	4060	0.80	0.03	1	1.8	−8.56	0.8	2.4
CI Tau	K7	4060	1.01	0.11	2	2.0	−7.95	0.8	1.7
CW Tau	K3	4730	1.32	0.05	2	1.7	−8.58	1.2	6.6
CX Tau	M2.5	3488	0.48	0.03	2	1.9	−8.18	0.3	0.8
CY Tau	M1	3705	0.55	0.04	1	1.8	−8.24	0.5	1.4
DE Tau	M2	3560	1.01	0.07	1	2.6	−7.69	0.4	0.2
DL Tau	K7	4060	0.89	0.23	2	1.9	−7.66	0.8	2.2
DM Tau	M1	3705	0.24	0.10	2	1.2	−7.99	0.5	3.6
DN Tau	M0	3850	0.91	0.02	1	2.2	−8.55	0.6	1.1
DO Tau	M0	3850	0.79	0.60	1	2.0	−7.10	0.6	1.3
DR Tau	K7	4060	1.09	0.72	2	2.1	−7.12	0.8	1.5
DS Tau	K2	4900	0.90	0.21	1	1.3	−8.00	1.1	17.0
FM Tau	M0	3850	0.26	0.10	2	1.2	−8.13	0.6	6.3
FZ Tau	M0	3850	1.06	0.46	3	2.3	−7.14	0.6	0.8
GM Aur	K3	4730	1.26	0.07	1	1.7	−8.44	1.2	7.2
GO Tau	M0	3850	0.27	0.01	3	1.2	−9.14	0.6	4.8
HO Tau	M0.5	3778	0.16	0.01	2	0.9	−9.13	0.5	8.7
IQ Tau	M0.5	3778	0.73	0.04	2	2.0	−8.24	0.6	1.2
RY Tau	K1	5080	6.59	1.60	4	3.3	−7.03	2.2	1.1
SU Aur	G2	5860	10.6	0.55	4	3.2	−7.52	1.7	2.2
UZ Tau E	M1	3705	2.27	0.31	2	3.7	−7.02	0.5	0.1

References. (1) Gullbring et al. (1998); (2) Valenti et al. (1993), these accretion luminosities have been multiplied by a factor of (140 pc/160 pc)^2 to account for the current estimate of 140 pc for the distance to the Taurus-Auriga star forming region; (3) Herczeg et al. (2009, in preparation); (4) Calvet et al. (2004).

minimizing the emission due to accretion, the typical selected colors are between the R and H bands. Since for some of the objects at later spectral types in our sample $R - I$ measurements are not available, we dereddened the $J - H$ and $H - K_s$ colors from the 2MASS All Sky Catalog of point sources[3] to the locus observed for classical T Tauri stars (CTTS) by Meyer et al. (1997), following the method described in Briceño et al. (2002). Extinctions are finally calculated adopting the extinction law of Rieke & Lebofsky (1985).

The computed photospheric luminosities cover a range from 0.16 $L_\odot$ (HO Tau) to 10.6 $L_\odot$ (SU Aur). Considering the uncertainties in the photometry, reddenings, bolometric corrections and distance, the typical errors in the bolometric luminosities are ±0.08−0.13 in log $L_\star$. Slight differences from the values obtained by other authors are typically within the uncertainties and are not significant for the purposes of this paper.

Given the effective temperatures and photospheric luminosities, we placed the PMS stars on the H-R diagram and derived stellar masses and ages adopting the theoretical tracks and isocrones of Palla & Stahler (1999) (see Fig. 2). One important source of uncertainty for stellar masses and ages is given by the spread of values obtainable by using different PMS evolutionary models. For example, compared to the ones obtained with the Baraffe et al. (1998) models, our adopted values of stellar masses and ages are typically lower by a factor of ~1.5 and ~2 respectively. Our choice of using the Palla & Stahler (1999) models is only due to the more complete coverage of the HR diagram plane, which allows us to use the same evolutionary models for all the sources of our sample. One should always bear in mind the high uncertainty associated to these quantities, expecially to the stellar age (see Sect. 4.1 for a more detailed discussion about

[3] For this analysis the JHK_s magnitudes have been transformed from the 2MASS photometric system to the Johnson-Glass one using the color transformations reported in Carpenter (2001) and Bessell & Brett (1988).
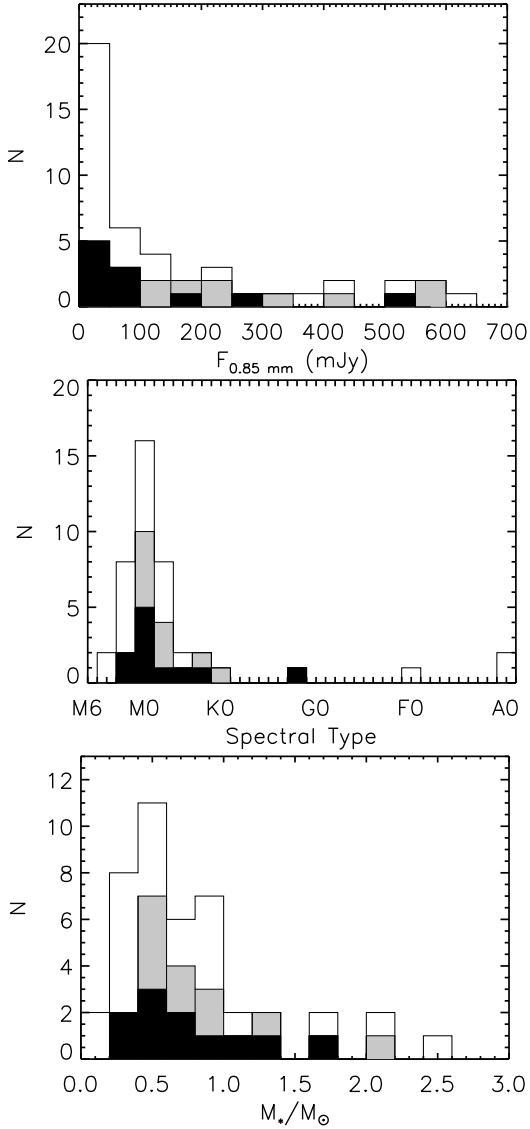
the estimates of YSO ages). According to the Palla & Stahler (1999) models the ranges spanned by our sample go from about 0.3 $M_\odot$ (CX Tau) to 2.2 $M_\odot$ (RY Tau) in stellar masses and from about 0.1 Myr (UZ Tau E) to 17 Myr (DS Tau) in stellar ages.

The main stellar quantities described here are summarized in Table 2.

2.4. Mass accretion rates

Given the stellar luminosities and effective temperatures we calculated the stellar radii using the Stefan-Boltzmann law. Once the stellar mass $M_\star$ and radius $R_\star$ are set, the mass accretion rate $\dot{M}_{\rm acc}$ can be directly obtained from an estimate of the accretion luminosity $L_{\rm acc}$ by

$$\dot{M}_{\rm acc} = 1.25 \frac{R_\star L_{\rm acc}}{GM_\star}, \qquad (1)$$

where G is the gravitational constant and the factor of ~1.25 is calculated assuming a disk truncation radius of ~5 $R_\star$ (Gullbring et al. 1998).

The estimates of $L_{\rm acc}$ were obtained from spectroscopic detections of excess Balmer continuum emission in the literature (see references in Table 2). These estimates are obtained primarily from measuring the excess flux in the Balmer continuum shortward of 3646 Å. The luminosity is then obtained by applying a bolometric correction calculated from shock models (Calvet & Gullbring 1998; Gullbring et al. 2000) or simplistic plane-parallel slabs (Valenti et al. 1993; Gullbring et al. 1998).

Two sources in our sample, FZ Tau and GO Tau, do not have literature estimates of accretion luminosity from the excess Balmer continuum emission. We obtained the accretion luminosity for these two sources from low-resolution spectra from 3200–8700 Å obtained with the double spectrograph at the 5m Hale Telescope at Palomar. The accretion luminosity was then

Fig. 2. H-R diagram for the sources of our sample. The dashed lines correspond to the isochrones for ages in Myr as labeled at the right end of the lines from the 1999 PMS evolutionary models, while the solid ones represent the evolutionary tracks from the same models for PMS stars with masses as labeled at the top of the evolutionary track lines. In this diagram the evolutionary tracks start from an age of 0.1 Myr. The errorbars for the ($T_{\rm eff}$, $L_\star$) values of our objects are not shown, the uncertainties in the photometric parameters are typically $\sim0.08-0.13$ in $\log L_\star$ and $\sim100–150$ K in temperature.

Table 3. Literature sources for the sub-mm/mm data.

λ (mm)	Source references
0.450	1
0.600	2, 3
0.624	4
0.769	4
0.800	2, 3
0.850	1, 5
0.880	5
1.056	4
1.100	2, 3
1.200	6
1.300	1, 7, 8, 9, 10
1.330	5
2.000	2, 11
2.700	7, 8, 12, 13
3.100	8
3.400	9, 14
7.000	15

References. (1) Andrews & Williams (2005); (2) Mannings & Emerson (1994); (3) Adams et al. (1990); (4) Beckwith & Sargent (1991); (5) Andrews & Williams (2007); (6) Althenoff et al. (1994); (7) Dutrey et al. (1996); (8) Jensen et al. (1996); (9) Koerner et al. (1995); (10) Isella et al. (2009); (11) Kitamura et al. (2002); (12) Mundy et al. (1996); (13) Schaefer et al. (2009); (14) Ohashi et al. (1996); (15) Rodmann et al. (2006).

Fig. 1. Histograms higlighting some properties of our selected sample. In all the histograms our sample is represented by black+grey columns, the black columns represent the disks in our sample for which we obtained new PdBI data at ~3 mm, while the total columns (black+grey+white) include all the class II YSOs from the Andrews & Williams (2005) catalog with no evidence of stellar companions in the 0.05−3.5″ interval in angular separation, from which our sample has been selected (see text). The *upper* histogram represents the distribution of the ~0.85 mm fluxes, including upper limits, for all the sources but two, 04113+2758 and GM Aur, which have not been observed at ~0.85 mm. *Middle and bottom* histograms show the distribution of stellar spectral type and estimated stellar mass (see Sect. 2.3) respectively. Four class II YSOs are not included in these histograms because for them an estimate of the stellar spectral type is not available. These are 04301+2608, FT Tau, Haro 6-39 and IC 2087.

calculated from the excess Balmer continuum emission, following the method described in Herczeg & Hillenbrand (2008).

2.5. Disks sub-mm and mm data from the literature

In order to probe the sub-millimetre and millimeter SED we collected data of the dust continuum emission between ~0.450 to ~7 mm from several works in the literature, listed in Table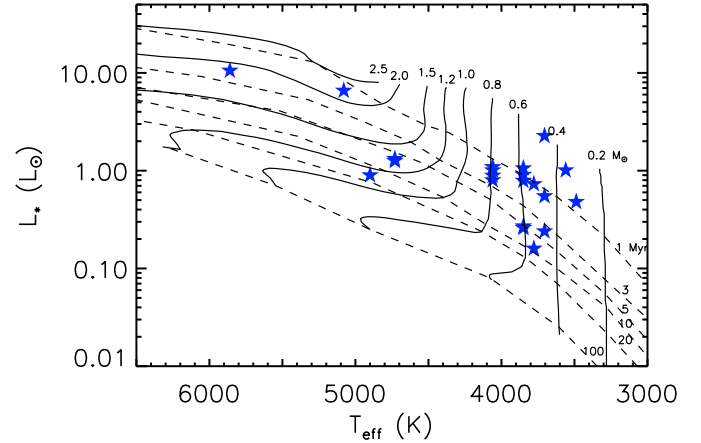 3. These data, except for 7 mm measurements, have been used together with the new PdBI observations at ~3 mm to constrain the disk properties by fitting the sub-mm/mm SED with the models described in Sect. 3. The 7-mm data are excluded because free-free emission from ionized gas contaminates disk emission, with free-free emission typically contributing ~20% of the 7 mm flux (Rodmann et al. 2006). Simultaneous cm observations are required to constrain the free-free emission at 7 mm, which is variable on short timescales ($\lesssim$ a few days, see Lommen et al. 2009). Only two disks in our sample (RY Tau and UZ Tau E) have been observed nearly simultaneously at centimeter and millimeter wavelengths (Rodmann et al. 2006), without which the 7 mm fluxes should be considered only as upper limits for the dust emission. We therefore did not include the 7 mm data in

our analysis, although we included the available 7 mm data from the literature in Fig. 4 and verified a posteriori that the fluxes of our disk models for all sources are equal or less than the measured flux at 7 mm. Simultaneous 7 mm and cm-wavelength observations with the EVLA will extend the coverage of the disk SED to longer wavelengths to better constrain the millimeter-wavelengths dust opacity and to provide information on dust grains larger than ~1 cm.

3. Disk models

We compare the observational sub-mm/mm data with the two-layer models of flared disks (i.e. in hydrostatic equilibrium) heated by the stellar radiation as developed by Dullemond et al. (2001), following the schematization of Chiang & Goldreich (1997). These models have been used in the analysis of CQ Tau by Testi et al. (2003) and of a sample of nine Herbig Ae stars by Natta et al. (2004) and we refer the interested reader to these papers for a more detailed description.

To completely characterize a model of the disk, we need to specify the stellar properties (i.e. the luminosity $L_\star$, effective temperature T_{eff}, mass $M_\star$ and distance d, assumed to be 140 pc for all the sources in our sample), some characteristics of the disk structure, namely the inner and outer radius (R_{in} and R_{out}, respectively), the parameters Σ_1 and p which define the radial profile of the dust surface density assumed to be a power-law[4] $\Sigma_{dust} = \Sigma_{dust,1}(R/1 \text{ AU})^{-p}$, the disk inclination angle i (90° for an edge-on disk) and, lastly, the dust opacity. The millimeter SED is almost completely insensitive to some of the disk parameters, which consequently cannot be constrained by our analysis. For example, the inner radius of the disk, R_{in}, affects the emission only at near and mid-infrared wavelengths.

The outer radius R_{out} is a parameter that can be probed by high-angular resolution interferometric observations. In our sample 13 disks have been spatially resolved, yielding an estimate for R_{out}. It is important to note that different interferometric observations performed on the same disk can lead to very different values of R_{out} (≥ 100 AU) because of differences in the observations' angular resolution, sensitivity, and methods for deriving the radius. Given these uncertainties in the determination of R_{out}, we consider a range of possible values for R_{out} rather than a single-value estimate, as listed in Table 4. For the eight objects in our sample that have not yet been mapped with angular resolutions smaller than a few arcseconds which may potentially resolve the disk, a fiducial interval of 100−300 AU has been assumed[5]. This adopted range for R_{out} comprises the vast

majority of the disk outer radii distribution function as derived by Andrews & Williams (2007) through ~1″ angular resolution sub-millimeter observations of 24 disks in Taurus-Auriga and ρ-Ophiucus. We will discuss the impact of the outer disk uncertainty on the results of our analysis in Sect. 4. Here we wish to note that with these values of R_{out} the disk emission at sub-mm/mm wavelengths is dominated by the outer disk regions ($R > 30$ AU) which are optically thin to their own radiation. An effect of this is that the millimeter SED does not depend on the disk inclination angle i (for $i \lesssim 80°$), thus decreasing the number of the model parameters used to fit the observational SED. This is certainly true for the spatially resolved disks for which we have an estimate for R_{out}. The eight unmapped objects could have optically thick inner disks that contribute significantly to the sub-mm/mm emission. Since the disk outer radius cannot be constrained by the SED alone, interferometric imaging that spatially resolves these disks is the only way to get information on the exact value of R_{out}. Nevertheless, since the disks that have been spatially resolved so far show outer radii typically in the range 100−300 AU, we consider it to be highly unlikely that a significant fraction of the unmapped disks have a $R_{out} \lesssim 50$ AU, which would make the disk optically thick even at mm wavelengths.

3.1. Dust opacity

The last quantity that defines the disk model is the dust opacity, which depends on grain sizes, chemical compositions, and shapes (e.g. Miyake & Nakagawa 1993; Pollack et al. 1994; Draine et al. 2006). In order to extract quantitative estimates from the sub-mm/mm SED for the dust grain sizes and the dust mass in the disks, assumptions on the chemical composition and shape of the dust grains have to be made.

For our discussion we considered porous composite spherical grains made of astronomical silicates, carbonaceous materials and water ice (optical constants for the individual components from Weingartner & Draine 2001; Zubko et al. 1996; Warren 1984 respectively) and adopted the fractional abundances used by Pollack et al. (1994) (see caption of Fig. 3). We considered a population of grains with a power-law size distribution $n(a) \propto a^{-q}$ between a minimum and a maximum size, a_{min} and a_{max}, respectively. In the ISM, a_{min} is a few tens of Å, $a_{max} \sim 0.1{-}0.2$ μm, and $q = 3.5$ (Mathis et al. 1977, Draine & Lee 1984, by analyzing extinction and scattering of starlinght from the interstellar dust). As discussed e.g. in Natta et al. (2004), in a protoplanetary disk one expects much higher values of a_{max} than in the ISM because of grain processing, and a variety of possible q values, depending on the processes of grain coagulation and fragmentation that occur in the disk. Experimental studies of fragmentation from a single target have found values of q ranging from ≈ 1.9 for low-velocity collisions to ≈ 4 for catastrophic impacts (Davies & Ryan 1990), but the power-law index for fragments from shattering events integrated over a range of target masses need not be necessarily the same as in the case of a single target. In the disk, if the coagulation processes from the initial ISM-grains population dominate over the fragmentation, a value for q that is lower than the ISM one is expected (the opposite should occur in the case of fragmentation playing the major role).

In the adopted two-layer disk model, the disk is divided into the surface and midplane regions, and therefore two different opacity laws are considered. Because of the assumed vertical hydrodynamical equilibrium and dust settling, the content of mass
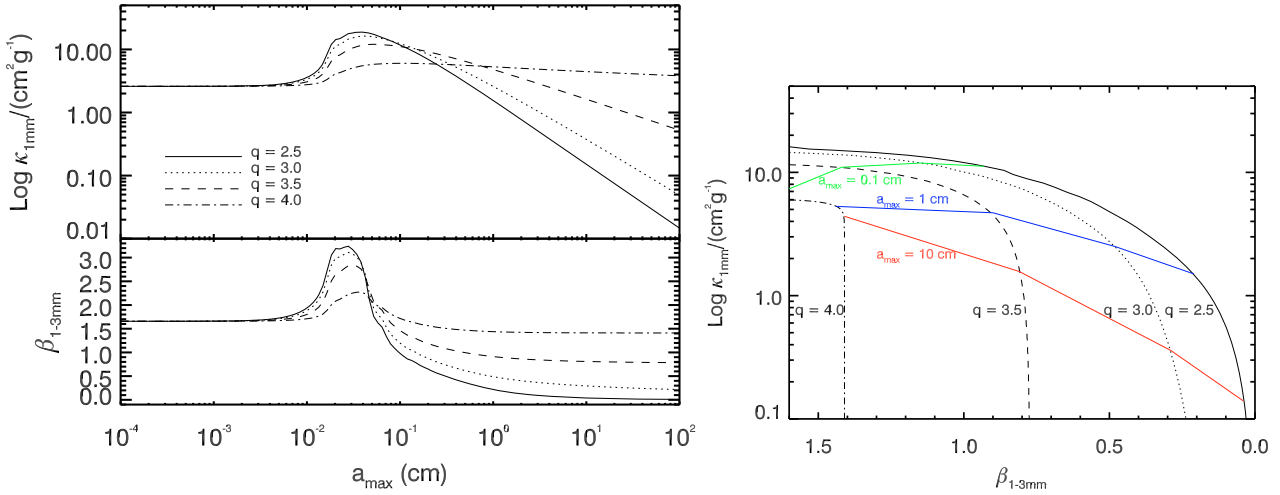
---

[4] As shown by Hughes et al. (2008) and Isella et al. (2009), a tapered exponential edge in the surface density profile, physically motivated by the viscous evolution of the disk, is able to explain the apparent discrepancy between gas and dust outer radii derived from millimeter observations of protoplanetary disks. Here we wish to note that when fitting the sub/mm-mm SED with an exponential tail instead of a truncated power-law, the dust opacity spectral index β (defined in Sect. 3.1) is unchanged, and disk masses vary by less than a factor of two, even if the outer disk radius becomes much bigger (see, e.g., Table 4 in Kitamura et al. 2002). So the simpler truncated power-law model is a justified approximation for the purposes of this paper.

[5] We will refer to these sources (CW, CX, DE, DS, FM, FZ, HO Tau, and SU Aur) as "unmapped" for the rest of the paper. Note that they are all faint with $F_{1 \text{ mm}} < 120$ mJy. This probably explains why for these objects no observations at high-angular resolution have been attempted yet: the sensitivity of the current (sub-)mm interferometers would be not high enough to detect the low surface brightness of the outer disk regions.

Fig. 3. Millimeter dust opacity for the adopted dust model. *Left top panel*: dust opacity at 1 mm as a function of a_{max} for a grain size distribution $n(a) \propto a^{-q}$ between $a_{min} = 0.1$ μm and a_{max}. Different curves are for different values of q, as labelled. The dust grains adopted here are porous composite spheres made of astronomical silicates ($\approx$10% in volume), carbonaceous materials ($\approx$20%) and water ice ($\approx$30%; see text for the references to the optical constants). *Left bottom panel*: β between 1 and 3 mm as a function of a_{max} for the same grain distributions. *Right panel*: dust opacity at 1 mm as function of β between 1 and 3 mm for the same grain distributions; different iso-a_{max} curves for $a_{max} = 0.1, 1, 10$ cm are shown. In the plots the unit of measure for the dust opacity is cm^2 per gram of dust.

in the midplane in a protoplanetary disk is much higher than in the surface. At millimeter wavelengths, where the disk is mostly optically thin to its own radiation, the midplane total emission dominates over that of the surface (although the surface dust plays a crucial role for the heating of the disk). As a consequence, we can extract information from our analysis only on the dust opacity of the midplane, and so when we consider the dust opacity we will refer only to the midplane component for the rest of the paper.

For the dust grains in the disk surface we assumed the same chemical composition and shape as for the midplane grains, while we assumed for their size distribution for a_{min} and a_{max} values around 0.1 μm (the sub-mm SED is insensitive to these values as long as a_{max} in the surface is much lower than a_{max} in the midplane, as expected if dust settling is important).

Once the chemical composition and shape of the dust grains in the midplane are set, the dust opacity law depends on a_{min}, a_{max} and q. Considering a value of 0.1 μm for a_{min} (the dependence of the millimeter dust opacity from this parameter turns out to be very weak), the model parameters for our analysis are the stellar parameters ($L_\star$, T_{eff}, $M_\star$), which have been set and listed in Table 2, plus those of the disk ($\Sigma_{dust,1}$, p, R_{out}, q, a_{max}), or equivalently (M_{dust}, p, q, a_{max}, R_{out}) where M_{dust} is the mass of dust in the disk.

For reasons described in Sect. 4 it is convenient to approximate the millimeter dust opacity law discussed so far in terms of a power-law at millimeter wavelengths $\kappa = \kappa_{1mm}(\lambda/1 \text{ mm})^{-\beta}$, with $\kappa_{1 mm}$ in units of cm^2 per gram of dust. At a fixed value of q the relations between $\kappa_{1 mm}$, β and a_{max} can be determined. These are shown in Fig. 3 for $q = 2.5, 3, 3.5, 4$.

4. Results

The sub-mm/mm SED fits for all the objects in our sample are reported in Fig. 4[6]. As discussed in Testi et al. (2003) and

Natta et al. (2004), the only quantities that can be constrained by the sub-mm/mm SED are the millimeter dust opacity spectral index β (in this paper calculated between 1 and 3 mm) and the $M_{dust} \times \kappa_{1 mm}$ product[7]. From the SED alone it is impossible to constrain the value of the surface density exponent p, since it is generally possible to fit the SED data with either very flat ($p = 0.5$) or very steep ($p = 2$) surface density profiles. However, all available high angular resolution observations performed so far suggest that $p \leq 1.5$ (e.g. Dutrey et al. 1996; Wilner et al. 2000; Kitamura et al. 2002; Testi et al. 2003; Andrews & Williams 2007; Isella et al. 2009; Andrews et al. 2009).

The degeneracy of the SED on p and R_{out} has an impact onto the derived uncertainties for β and $M_{dust} \times \kappa_{1 mm}$. Considering both this degeneracy and uncertainties of the observational data, the total absolute uncertainties are approximately 0.2−0.3 for β and a factor of $\approx$ three and $\approx$ four for $M_{dust} \times \kappa_{1 mm}$ for the spatially resolved and unmapped disks respectively. These uncertainties are mainly due to the adopted ranges for R_{out} (listed in Table 4) and p between 0.5 and 1.5, whose values determine the impact of the optically thick regions of the disk to the total emission, as explained in Sect. 3.

The estimates for β and $M_{dust} \times \kappa_{1mm}$ obtained by our analysis are reported in Table 5.

4.1. Spectral slopes and dust opacity index

Before analysing the values of β, which provide information on the level of grain growth in the outer disk regions, it is important to check whether our results could be affected by detection biases: indeed, for a given flux at ~1 mm, a disk with large

---

[6] We did not include existing NIR and mid-IR data in our analysis because at these shorter wavelengths the disk emission is optically thick

and thus depends on the properties of the dust grains located in the surface layers of the inner disk regions. The aim of our analysis is instead to probe the optically thin disk emission to investigate the dust properties in the disk midplane.

[7] Note that according to the adopted disk model the midplane temperature is well constrained after fixing the stellar parameters and these two quantities from the observed SED.
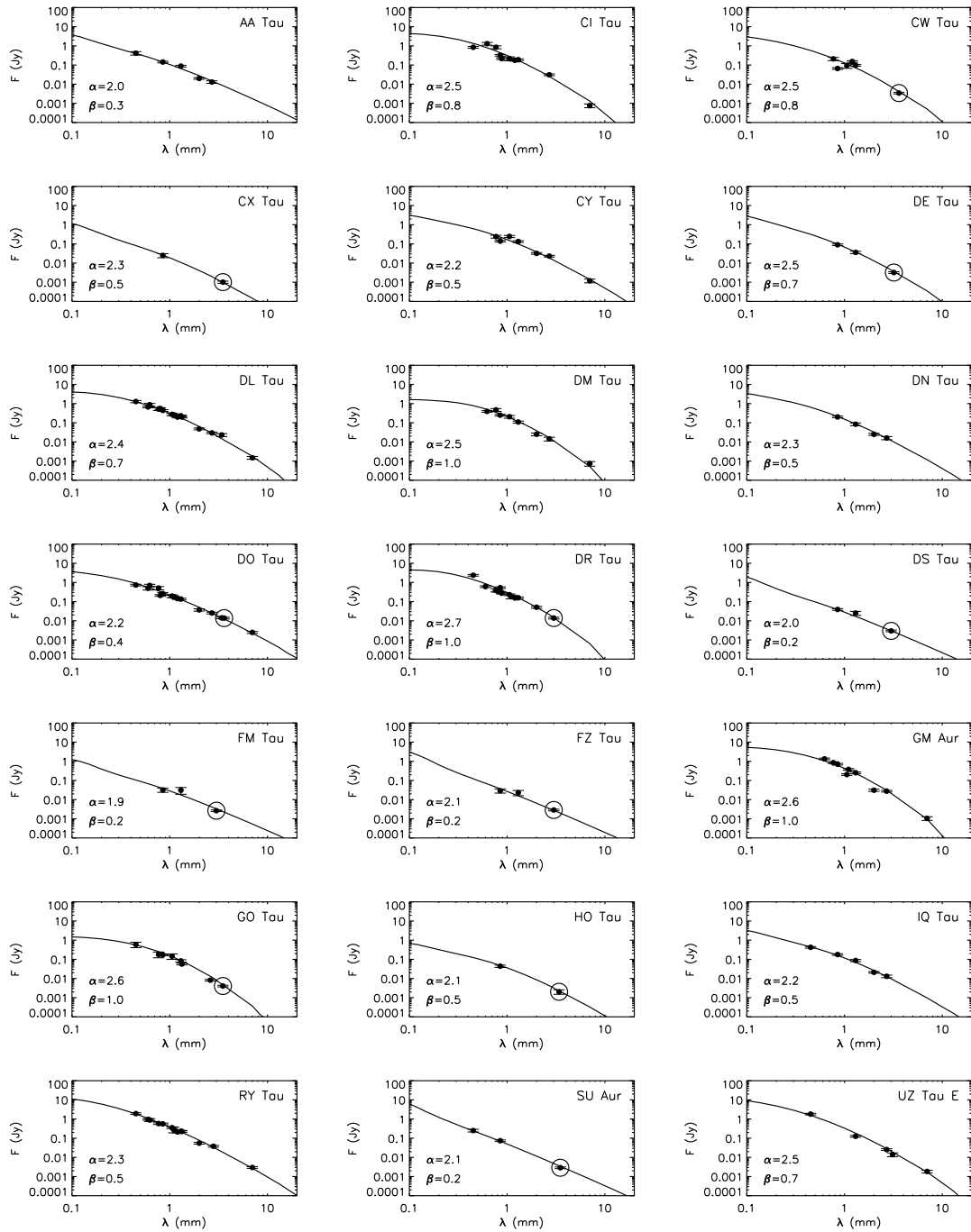
Fig. 4. Fits of the sub-mm/mm SEDs with the two-layer flared disk models (solid lines). Note that even if the data at 7 mm, available for only eight disks in our sample, are present in the plots, they have not been used in the fitting procedure (see Sect. 2.5). The errorbars in the plots take into account an uncertainty of 10% on the absolute flux scale, typical for flux measurements at these wavelengths. The circled data come from the new PdBI observations. The fitting values of the spectral index α and of the dust opacity spectral index β between 1 and 3 mm are indicated in the bottom left corner of each plot. The value of the surface density power-law index p adopted in these fits is 1, and the adopted value for the outer disk radius is listed in Table 5.

dust grains in the outer parts will produce a stronger emission at ~3 mm than a disk with a population of smaller-sized grains and it would be easier to detect. In Fig. 5 the grey region of the plot indicates the area in the ($F_{1\,mm}$, α_{1-3mm}) plane in which the observations carried out so far are not sensitive, due to the sensitivity limits obtained at 1 and 3 mm. While we could investigate the dust properties for four disks with 15 mJy < $F_{1\,mm}$ < 30 mJy, the plot shows that a disk with a 1 mm flux in this same range,

but with a spectral index $\alpha_{1-3\,mm} \gtrsim 3.2$, which is consistent with a disk model with ISM-like dust and an outer radius of ~100 AU, would not be detected at 3 mm. Nevertheless, we want to point out that only two of our 16 targets with $F_{1\,mm}$ < 100 mJy were not detected at 3 mm, and both have very weak $F_{1.3\,mm}$ fluxes (upper limits of 27 mJy and 21 mJy for DP Tau and GK Tau respectively, Andrews & Williams 2005), therefore the lack of disks with α ~3.2 at $F_{1\,mm}$ > 30 mJy does not seem to be

Table 4. Adopted disk outer radii.

Object	R_{out}^a (K02) (AU)	R_{out}^a (AW07) (AU)	R_g^b (I09) (AU)	Adopted R_{out}-interval (AU)
AA Tau	214^{+63}_{-51}	400^{+600}_{-75}	...	200−400
CI Tau	...	225 ± 50	...	150−250
CW Tau	...	...	...	100−300
CX Tau	...	...	...	100−300
CY Tau	211 ± 28	...	230	230−330
DE Tau	...	...	...	100−300
DL Tau	152^{+28}_{-27}	175^{+50}_{-25}	...	150−250
DM Tau	220 ± 47	150^{+250}_{-100}	160	160−260
DN Tau	147 ± 469	100^{+300}_{-25}	125	125−225
DO Tau	98 ± 52	...	...	100−200
DR Tau	193 ± 141	100^{+175}_{-25}	90	90−190
DS Tau	...	...	...	100−300
FM Tau	...	...	...	100−300
FZ Tau	...	...	...	100−300
GM Aur	151^{+63}_{-29}	150 ± 25	270	270−370
GO Tau	...	350^{+650}_{-175}	160	160−260
HO Tau	...	...	...	100−300
IQ Tau	329^{+403}_{-70}	...	...	250−400
RY Tau	81 ± 128	150 ± 25	115	115−215
SU Aur	...	...	...	100−300
UZ Tau E	...	...	160	160−260

Notes. $^{(a)}$ R_{out} listed here results from image fitting using a truncated power-law for the surface density profile. K02: Kitamura et al. (2002); AW07: Andrews & Williams (2007). $^{(b)}$ R_g is the radius within which the 95% of the flux is observed, after fitting the visibility of the source with a Gaussian; we used this value, when available, as a lower limit for our adopted R_{out}-interval. I09: Isella et al. (2009).

due to our sensitivity limit, but is most likely real. Furthermore, as is evident from the same plot, the six faintest disks with $F_{1\,\mathrm{mm}} < 60$ mJy show a spectral index between 1 and 3 mm that is lower on average (2.08 ± 0.08) than for the brighter disks (2.40±0.06). This is the reason for the discrepancy of the average value of the dust opacity spectral index $\langle \beta \rangle$ between unmapped and resolved disks (see discussion below).

In Fig. 3 we plot $\kappa_{1\,\mathrm{mm}}$ and β as functions of a_{max} for different values of q. One interesting result is that the values of β obtained for the objects in our sample by the SED-fitting procedure are all less than or equal to 1, which can be explained only if dust grains with sizes larger than 1 mm are present in the disk. For the nine sources with $\beta \leq 0.5$, the largest dust grains must have grown to sizes ≥1 cm according to our dust model. If we let q assume values lower than 2.5, thus increasing the fractional number of the larger grains, the maximum grain size decreases, but $a_{\mathrm{max}} \gtrsim 1$ mm for $\beta \lesssim 1$ is still needed.

The estimates of the maximum grain sizes a_{max} depend on the adopted dust model. If we consider for example the dust model adopted in Natta et al. (2004) (5% olivine, 15% organic materials, 35% water ice and 50% vacuum), the estimates for a_{max} are greater by about an order of magnitude than the ones obtained with our dust model. In general, no realistic dust grain models result in $\beta < 1$ for $a_{\mathrm{max}} < 1$ mm.

Here it is worthwhile to remember that whereas for the 13 resolved disks in our sample β is well determined, for the eight disks for which we do not have information on their spatial extension, the optically thick parts of a possible compact disk could significantly contribute to the emission. If that is the case, no conclusions on the dust grain properties could be drawn. In particular, for the six unmapped disks with $\alpha \approx$ 1.9−2.2 (CX Tau, DS Tau, FM Tau, FZ Tau, HO Tau, SU Aur) a very compact disk with $R_{\mathrm{out}} \approx 20$ AU, a relative high inclination $i \approx 70°$, and

with ISM-like dust grains would fit the sub-mm/mm SED. For the other two unmapped sources, DE Tau ($\alpha \approx 2.4$) and CW Tau ($\alpha \approx 2.5$), ISM-like dust grains are consistent with the sub-mm/mm data using a disk model with $i \approx 70°$ and $R_{\mathrm{out}} \approx 30$, 40 AU respectively. For the faintest disks the outer radius has to be small, because if the disks were larger they would also need to be more massive to keep being optically thick, thus producing an α value close to 2 with all the possible dust properties. In that case, they would emit more sub-mm/mm-wave radiation than observed. Since for an optically thick disk decreasing the inclination angle has the effect of making the SED steeper (because the central, hotter parts are less obscured), for disks with $i < 70°$ the outer radii would need to be even smaller to fit the SED. As these disk outer radii are lower by factors of 2−4 than the smallest disks that have been spatially resolved so far, and since for all the 13 resolved disks the values of β have been found always much lower than in the ISM ($\beta_{\mathrm{ISM}} \approx 1.7$, see Fig. 6), thus showing clear evidence of grain growth, we consider it to be very unlikely that many of the unmmapped sources are compact, optically-thick disks with unprocessed ISM grains. For AA Tau, which is the faintest of the mapped sources ($F_{1\,\mathrm{mm}} \approx 100$ mJy) and which has a low spectral index of $\alpha \approx 2.0$ typical of fainter sources, the maps indicate a disk radius of 200−400 AU, ruling out the possibility of optically thick disk regions that dominate the total emission, and require a low β of 0.3 to explain the shallow slope.

Also, only for the disks with $\beta \gtrsim 0.8$, values of $q \gtrsim 3.5$ are consistent with the data (see right panel in Fig. 3), in which case $a_{\mathrm{max}} \geq 10$ cm. This agrees well with the following consideration using the approximated asymptotic formula $\beta \approx (q - 3)\beta_{\mathrm{RJ}}$, derived by Draine (2006), where β_{RJ} is the opacity spectral index of the solid material in the Rayleigh limit and is valid for a population of grains with $3 < q < 4$ and $a_{\mathrm{min}} \ll a_c \ll a_{\mathrm{max}}$,

with a_c a function of the real and imaginary parts of the complex dielectric function and wavelength (at millimeter wavelengths $a_c \sim 1$ mm). Since at a fixed q the function $\beta(a_{max})$ decreases when $a_{max} \gtrsim 1$ mm (see Fig. 3), it follows that the approximated asymptotic value $(q - 3)\beta_{RJ}$ gives a lower limit for β at a finite a_{max}. Adopting $\beta_{RJ} = 1.7$ from the small dust grains in the ISM, we derive $\beta \gtrsim 0.85$ for $q \gtrsim 3.5$, i.e. dust grain populations with $q \gtrsim 3.5$ cannot explain β-values lower than ≈ 0.85[8].

In Fig. 6 we report the histogram of the β-values derived by our analysis. The average value in our sample considering both unmapped and resolved disks, $\langle\beta\rangle = 0.6 \pm 0.06$, is not consistent with dust populations with q-values of 3.5, like for the ISM, or greater. Values of q lower than 3.5 have been obtained by e.g. Tanaka et al. (2005) from simulations of grain growth in stratified protoplanetary disks, which give vertically integrated size distributions with $q \approx 3$ plus a population of much larger bodies, to which however our observations would not be sensitive.

These considerations clearly suggest that the process of dust grain growth to mm-sizes has played a fundamental role in most, if not all, of the Taurus-Auriga protoplanetary disks whose sub-mm/mm SED has been sufficiently investigated.

From Fig. 6 it is also evident that the two sub-samples made of unmapped and resolved disks separately have different averaged β values, with the β values being on average lower for the unmapped disks than for the resolved ones ($\langle\beta\rangle = 0.41 \pm 0.10$, 0.68 ± 0.06 for the unmapped and resolved disks respectively). Since the unmapped sample nearly coincides with the fainter disks with $F_{1\,mm} < 100$ mJy, and since β is correlated with the spectral index α, this is due to the trend already presented in Fig. 5 between $F_{1\,mm}$ and $\alpha_{1-3\,mm}$. This trend agrees with simple expectations for grain growth: as the maximum grain size a_{max} increases, both β and $\kappa_{1\,mm}$ decrease, so disks with the same dust mass should become fainter as β gets smaller. Alternatively, the $F_{1\,mm}$-$\alpha_{1-3\,mm}$ trend could arise if the fainter disks are smaller, and then more optically thick, than the brighter resolved ones, while their "true" β would be nearly the same.

In Fig. 7 we show the β vs. stellar age plot. No evidence of an evolutionary trend is present over the broader range of stellar ages spanned by our sample. As already discussed the determination of the individual ages of PMS stars is very uncertain. Hartmann (2001) has shown that the large age spread deduced for T Tauri stars in Taurus may just be the result of uncertainties in the measurements towards individual members of a population with a very narrow age spread. Our most solid conclusion, not affected by the age determination uncertainties, is that most (if not all) of the class II YSO in our sample show evidence of evolved grains in the disk outer regions.

4.2. Grain growth

These results confirm two statements that have been addressed in the last years. The first one is that the dust coagulation from ISM dust to mm/cm-sized grains is a fast process, which appears to occur *before* a YSO enters in the class II evolutionary stage, i.e. when a dense envelope still surrounds the protostar+disk system. This is also consistent with the recent results by Kwon et al. (2009) who have found evidence of grain growth in three class 0 YSOs in Perseus and Cepheus through CARMA observations at 1.3 and 2.7 mm.

The second statement is that the mm/cm-sized dust grains appear to stay longer in the outer disk if compared with their
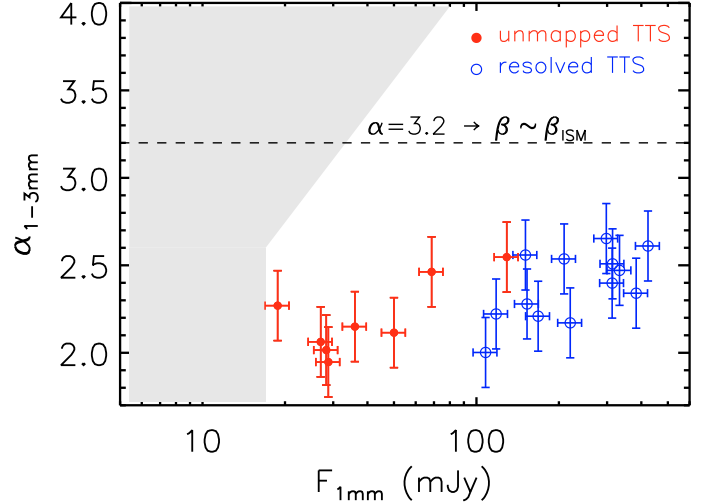

Fig. 5. Spectral index α between 1 and 3 mm plotted against the flux at 1 mm from the model best-fits shown in Fig. 4. The points plotted here are listed in the first two columns of Table 5. Open blue points represent the spatially resolved disks, whereas the filled red points are for the unmapped ones. A value of α consistent with a disk model with ISM-like dust and an outer radius of ~100 AU is indicated as a dashed horizontal line. The grey region shows the area in the plot that is unexplored because of the 3σ sensitivity limits of our new and past millimeter observations (here considered as 15 mJy and 1.0 mJy at 1 and 3 mm respectively).
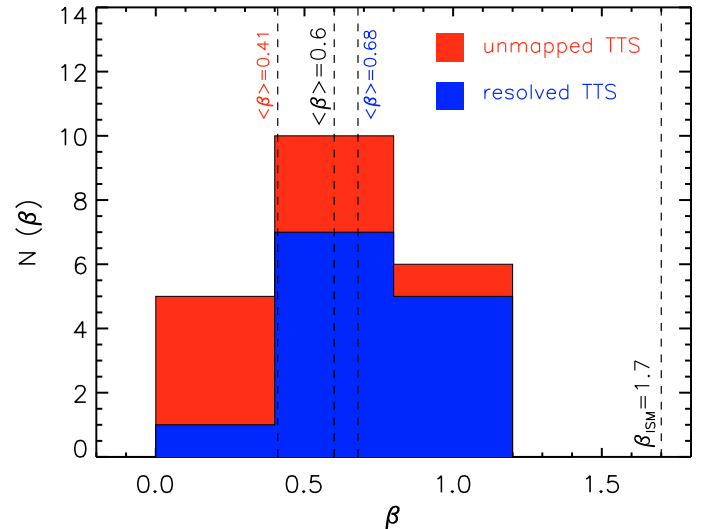

Fig. 6. Distribution of the dust opacity spectral index β for the disks in our sample. In blue are indicated the values for the spatially resolved disks, whereas the red is for the unmapped ones. The average β value for all the sources in our sample (black), for the unmapped sources only (red), for the resolved sources only (blue), and the value of 1.7 for the ISM dust are indicated as dashed vertical lines.

expected inward drift timescale due to the interaction with the gas component. In a circumstellar disk the gas experiences a pressure gradient force which cancels a part of the central star's gravity and induces a rotation slower than the Keplerian velocity. Dust grains, whose orbits are hardly affected by gas pressure, are assumed to be rotating with Keplerian velocity and thus experience a headwind. They lose angular momentum and spiral inward to the central star (Adachi et al. 1976; Weidenschilling 1977). Takeuchi & Lin (2005) proposed as possible solutions to the drift problem that either the grain growth process from
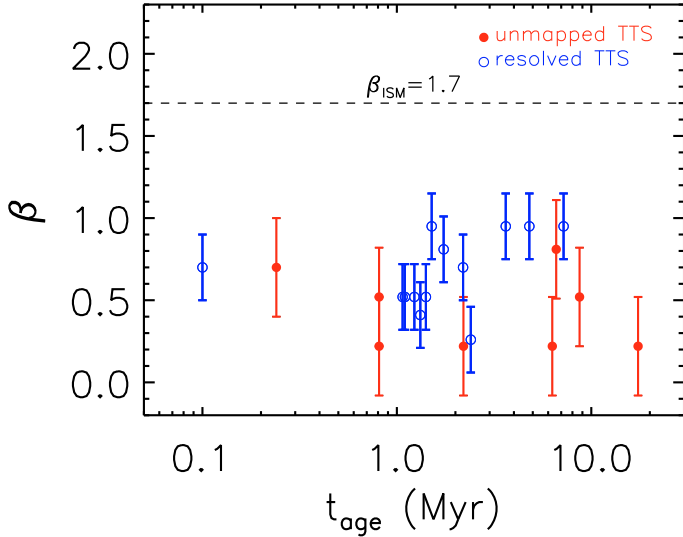
---

[8] Note that β-values greater than ≈ 0.85 can be explained by both $q \lesssim 3.5$ and $q \gtrsim 3.5$.

mm-sized to cm-sized grains is very long in the outer regions of the disk (timescales greater than 1 Myr, e.g. given by grains' sticking probability as low as 0.1) or that grains have already grown to 10 m or larger and do not migrate rapidly anymore, while mm-sized particles are continuosly replenished through collisions of these large bodies. However, our analysis suggests that unless the grain size distribution index is very low, i.e. $q < 2.5$, disks with $\beta \lesssim 0.5$ show evidence of grains as large as ~1 cm in the outer regions. Also, as already pointed out in Natta et al. (2004) and Brauer et al. (2007), a considerable amount of larger bodies, which would not contribute to the disk emission because of their negligibly small opacity coefficient, could significantly increase the disk masses. Since the typical orbital decay time for a cm-sized grain with a density of 0.1 g cm^{-3} at 50 AU is $\approx 10^5$ yr (10^4 yr for a more compact grain with a 1 g cm^{-3} density), to explain the presence of cm-sized grains in the older disks in our sample (with ages of few Myrs and up to $\sim 10^7$ yr) the reservoir of larger bodies would have to contain at least 100 times more mass than the observed dust mass. The total disk mass would then be comparable to or would even exceed the estimated stellar mass (using a standard gas-to-dust mass ratio of 100, see Sect. 4.3).

To solve the drift problem for very low and very high disk masses Brauer et al. (2007) proposed a significant reduction of the drag experienced by the dust due to a reduction of the gas-to-dust ratio in the disk from the canonical value of 100, and to possible collective effects of dust gathering in a thin midplane layer in the case of very low-turbulence disks. For example, using a low value for the turbulence parameter $\alpha = 10^{-6}$ and a gas-to-dust ratio of 5, they find that cm-sized dust grains remain in the outer parts of the disk for more than 2 Myr if disk masses $< 0.05 M_\star$ or $> 0.2 M_\star$ are considered. In the range of $M_{disk} \approx 0.05 - 0.2 M_\star$ the collective effects of dust are not efficient enough to retain cm-sized grains in the disk outer regions. If the disk is more turbulent, then more gas has to be removed to keep the particles in the outer parts for a longer period of time. To justify such small gas-to-dust ratios the authors suggest the process of photoevaporation as the main driver of gas removal. However, in this case, since photoevaporation is expected

to manifest only in the later stages of disk evolution, we would expect a strong evolutionary trend of β, which is not found by our analysis though.

Another possibility is the presence in the disk of local gas pressure maxima that would block the inward drift of the dust grains. As shown by the dynamics calculation of Barge & Sommeria (1995) and Klahr & Henning (1997), this mechanism may provide a solution also to the relative velocity fragmentation barrier that prevents meter-sized bodies to further grow in size in the inner regions of the disk.

4.3. Dust mass

From the sub-mm/mm SED fitting procedure we derived the quantity $M_{dust} \times \kappa_{1\ mm}$. To obtain the dust mass in the disks, an estimate of $\kappa_{1\ mm}$ is needed. The choice of the dust opacity at 1 mm creates the highest uncertainty in the derivation of (dust) disk masses from millimeter observations. Estimates of $\kappa_{1\ mm}$ from different dust models in the literature span a range of a factor greater than ten. The most commonly used value in the literature is $\kappa_{1\ mm} \simeq 3$ cm^2 per gram of dust (Beckwith et al. 1990) that, for simplicity, is supposed to be constant, i.e. independent of the dust grain properties, for all the disks. As noted in Natta et al. (2004) this is not realistic as grain growth affects both the frequency dependence of the dust opacity and its absolute value (e.g. Miyake & Nakagawa 1993).

In this paper we use the dust model described in Sect. 3.1 to get an estimate of $\kappa_{1\ mm}$ that takes into account the dust physical properties, expecially grain growth. As shown in the left top panel of Fig. 3, at a fixed value of the grain size distribution index q, the value of $\kappa_{1\ mm}$ can be inferred from a_{max} which in turn can be derived from β through the relation plotted in the left bottom panel of the same figure. The relation between κ_{1mm} and β is shown in the right panel. Therefore, from an estimate of β and $M_{dust} \times \kappa_{1\ mm}$ obtained by the sub-mm/mm SED fitting procedure we can get an estimate for κ_{1mm} and then the dust mass M_{dust} for our dust model, after fixing the q parameter. In Table 5 we report the values of M_{dust} as obtained with this method for $q = 2.5$, 3.0, 3.5. It is important to bear in mind that, as for the estimate of the maximum grain size, so also for κ_{1mm} and for the dust mass, the estimates depend on the specific dust model that one adopts (see discussion in Natta et al. 2004). However, following Isella et al. (2009), we take into account the variation of the dust opacity with β using a well defined dust model to infer dust masses, and this approach is more accurate than considering a fixed κ_{1mm}, as is often done in previous studies.

In general for our specific dust model, when $\beta < 1$ then $M_{dust}^{q=2.5} < M_{dust}^{q=3} < M_{dust}^{q=3.5}$, and the amount of variation of M_{dust}^q for the different q values is dependent on β. This is particularly the case when $\beta \simeq 0.8 - 1$ $M_{dust}^{q=2.5}$ and $M_{dust}^{q=3}$ are nearly coincident, and $M_{dust}^{q=3.5}$ is greater than $M_{dust}^{q=2.5}$ by factors of $\sim 2 - 4$. For $\beta \lesssim 0.7$ a grain size distribution with $q = 3.5$ cannot explain the observational data, and the discrepancy between $M_{dust}^{q=2.5}$ and $M_{dust}^{q=3}$ increases to a factor of ~ 15 when $\beta \simeq 0.2$. This is due to the increase of the distance between the $\kappa_{1\ mm}(\beta)$ curves at fixed q-values when β decreases, as shown in the right panel of Fig. 3.

As already mentioned in Sect. 4.1, from the value of β it is impossible to disentangle a_{max} and q. Nevertheless, only the disks showing $\beta \geq 0.8$ can be explained by a grain size distribution index $q = 3.5$. Consequently, we will separately consider for the rest of our analysis only those cases where the dust grain size distribution is characterized by $q = 2.5$ or 3. The value of q

Table 5. Disk properties.

Object name[a]	$R_{\rm out}^{b}$ (AU)	$F_{1\ \rm mm}^{c}$ (mJy)	$\alpha_{1-3\rm mm}$	$\beta_{1-3\rm mm}$	$M_{\rm dust} \times \kappa_{1\rm mm}$ ($M_\odot \times$ cm^{2}g^{-1})	$M_{\rm dust}^{q=2.5}$ ($M_\odot$)	$M_{\rm dust}^{q=3}$ ($M_\odot$)	$M_{\rm dust}^{q=3.5}$ ($M_\odot$)
AA Tau	300	108	2.0	0.3	2.8×10^{-4}	1.5×10^{-4}	1.5×10^{-3}	...
CI Tau	200	314	2.5	0.8	7.9×10^{-4}	1.1×10^{-4}	1.2×10^{-4}	5.0×10^{-4}
CW Tau	200	129	2.5	0.8	3.2×10^{-4}	4.2×10^{-5}	4.4×10^{-5}	1.9×10^{-4}
CX Tau	200	19	2.3	0.5	5.7×10^{-5}	1.2×10^{-5}	1.9×10^{-5}	...
CY Tau	280	168	2.2	0.5	6.0×10^{-4}	1.3×10^{-4}	2.0×10^{-4}	...
DE Tau	200	69	2.5	0.7	1.6×10^{-4}	2.4×10^{-5}	2.8×10^{-5}	...
DL Tau	200	313	2.4	0.7	8.4×10^{-4}	1.3×10^{-4}	1.5×10^{-4}	...
DM Tau	210	209	2.5	1.0	9.2×10^{-4}	1.0×10^{-4}	1.0×10^{-4}	1.6×10^{-4}
DN Tau	175	153	2.3	0.5	3.5×10^{-4}	7.7×10^{-5}	1.2×10^{-4}	...
DO Tau	150	220	2.2	0.4	4.9×10^{-4}	1.4×10^{-4}	3.1×10^{-4}	...
DR Tau	140	298	2.7	1.0	6.6×10^{-4}	7.4×10^{-5}	7.2×10^{-5}	1.2×10^{-4}
DS Tau	200	28	2.0	0.2	6.2×10^{-5}	4.0×10^{-5}	1.1×10^{-3}	...
FM Tau	200	29	1.9	0.2	6.5×10^{-5}	6.0×10^{-5}	1.7×10^{-3}	...
FZ Tau	200	27	2.1	0.2	5.0×10^{-5}	3.2×10^{-5}	9.0×10^{-4}	...
GM Aur	320	423	2.6	1.0	1.4×10^{-3}	1.6×10^{-4}	1.5×10^{-4}	2.5×10^{-4}
GO Tau	210	151	2.6	1.0	6.3×10^{-4}	7.1×10^{-5}	6.9×10^{-5}	1.1×10^{-4}
HO Tau	200	36	2.1	0.5	1.7×10^{-4}	3.7×10^{-5}	5.6×10^{-5}	...
IQ Tau	325	118	2.2	0.5	3.4×10^{-4}	7.4×10^{-5}	1.1×10^{-4}	...
RY Tau	165	383	2.3	0.5	5.1×10^{-4}	1.1×10^{-4}	1.7×10^{-4}	...
SU Aur	200	50	2.1	0.2	5.0×10^{-5}	3.2×10^{-5}	9.0×10^{-4}	...
UZ Tau E	210	333	2.5	0.7	6.1×10^{-4}	9.6×10^{-5}	1.1×10^{-4}	...

Notes. [a] Underlined objects are those that have not been mapped to date through high-angular resolution imaging. [b] Central value of the adopted $R_{\rm out}$-interval reported in Table 4. This is the value used to extract the other quantities listed in the Table. [c] Source flux density at 1 mm from the best fit disk model described in Sect. 3.

in protoplanetary disks is unknown and it is not observationally constrainable, and so it is in principle possible that it can vary substantially from one disk to the other. For our discussion we will use the assumption that q is the same for all the disks.

Once the dust mass is estimated, this is commonly converted into an estimate of the total disk mass (dust+gas) using the standard ISM gas-to-dust ratio of 100. However, if the dust and gas components have different evolutionary timescales, this ratio is a function of time, and the standard ISM value would be inappropriate to estimate the disk mass at the present time. Physical processes that are likely to alter this ratio during the evolution of a protoplanetary disk are gas photo-evaporation, which would lead to a decrease of the gas-to-dust ratio (unless a significant amount of dust is dragged away by the gas flow), and dust inward migration, which instead would increase it. Natta et al. (2004) suggested that the standard ISM ratio provides a correct estimate of the "original" disk mass when the disk composition reflects that of the parent cloud. This is only true however if a negligible amount of dust has migrated with respect to the gas and accreted onto the central star, otherwise the ISM ratio would provide only a lower limit to the original disk mass. Because of our ignorance on the gas-to-dust ratio evolution we will not convert the dust mass into a total disk mass. It is also important to note that since millimeter observations are insensitive to the emission of bodies much larger than 1 cm, including planetesimals and planets, the dust mass we are referring to in this paper does not include the contribution from these larger objects. The dust mass is intended to be the mass in "small grains" only, and is a lower limit to the total mass in dust.

Figure 8 shows the β vs. $M_{\rm dust}$ plots for q equal to 2.5 and 3. The plot with $q = 2.5$ does not show any significant relation. In the $q = 3$ case an anticorrelation between these two quantities may be present, with the more massive dust disks associated to the ones showing today the largest grains in their outer parts, with $a_{\rm max}$ up to ~10 cm. This possible anticorrelation is clearly an effect of the choice of a physical model for the dust that takes into account the variation of the dust opacity normalization factor with the size-distribution of the dust grains (Sect. 3.1). If we had made the unrealistic assumption of a constant value for the dust opacity at, say, 1 mm, we would have found an opposite result, i.e. disks with *less* mass in dust would have shown on average larger grains, as can be derived from Fig. 5, since α is approximately proportional to β and $F_{1\ \rm mm}$ would be approximately proportional to the dust mass in the constant $\kappa_{1\ \rm mm}$ case. More realistically, lower values of β imply low absolute values of the dust millimeter opacity (see right panel of Fig. 3), so that for a fixed observed flux and disk temperature, the corresponding dust mass must be larger. The reason why the plot with $q = 2.5$ does not show signs of anticorrelation is that at a fixed β a lower q value is associated to a smaller dust grain maximum size. The β range spanned by the disks in our sample translates into a range in $\kappa_{1\ \rm mm}$ that is narrower for $q = 2.5$ than it is for $q = 3$ (see right panel of Fig. 3), thus leading to smaller correction factors with respect to the constant $\kappa_{1\ \rm mm}$ case. Note that among the five disks showing the smallest β (≈ 0.2–0.3) and the highest dust masses (about 10^{-3} $M_\odot$ for $q = 3$) only one (AA Tau) has been mapped and spatially resolved. High angular resolution and high sensitivity imaging of these disks together with other ones are needed
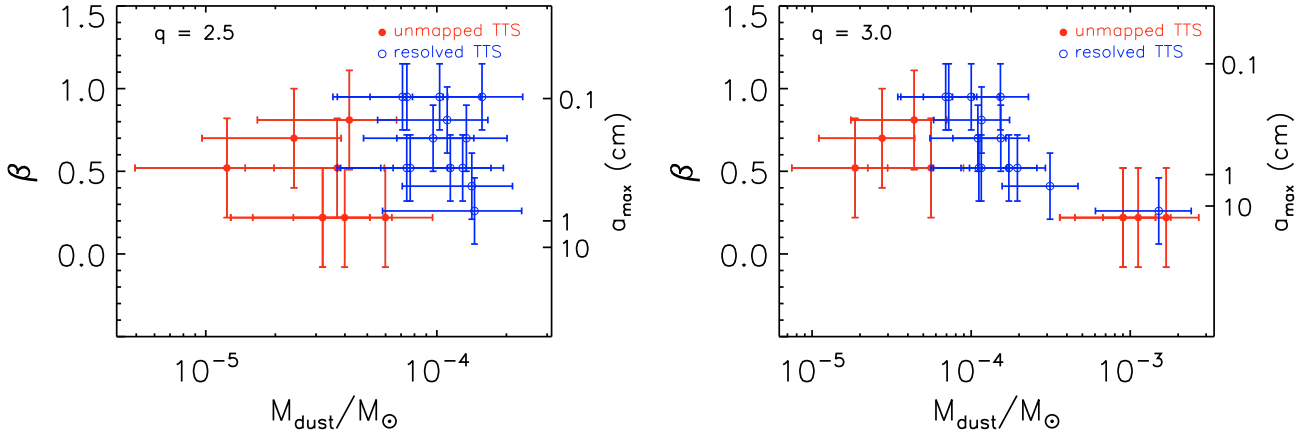
Fig. 8. Dust opacity spectral index β and maximum grain size a_{max} plotted against the disk mass in dust for the sources in our sample. In the *left and right panels* the dust mass has been obtained adopting a value of 2.5 and 3 respectively for the power index q of the dust grain size distribution. Open blue points represent the spatially resolved disks, whereas the filled red points are for the unmapped ones. The errorbars in the dust mass estimates do not take into account our uncertainty on the real value of q.
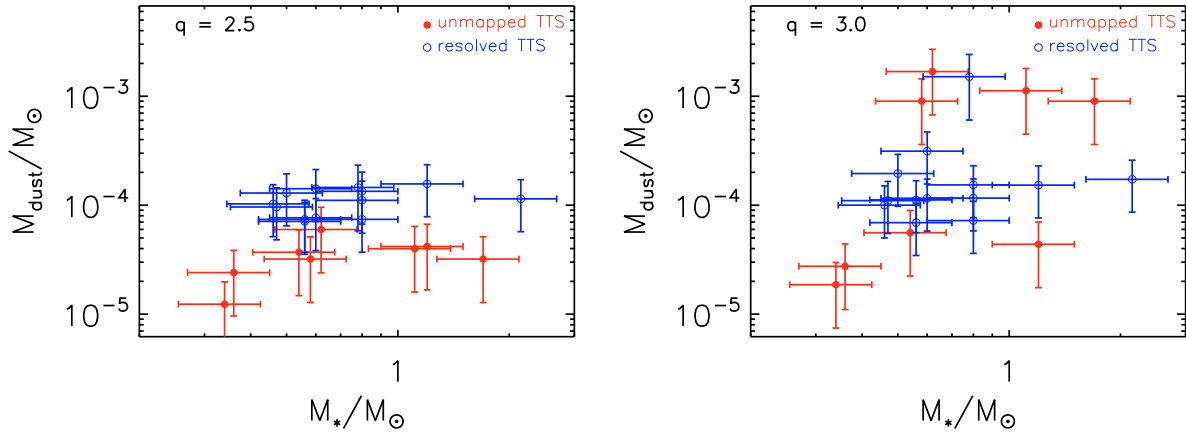
Fig. 9. Disk mass in dust plotted against the stellar mass for the sources in our sample. In the *left and right panels* the dust mass has been obtained adopting a value of 2.5 and 3 respectively for the power index q of the dust grain size distribution. The stellar mass has been estimated as described in Sect. 2.3, and the errorbars take into account the range of values given by different PMS stars evolutionary models. Open blue points represent the spatially resolved disks, whereas the filled red points are for the unmapped ones. The errorbars in the dust mass estimates do not take into account our uncertainty on the real value of q.

to test the robustness of the $\beta - M_{dust}$ anticorrelation in the $q = 3$ case.

Figures 9 and 10 plot the disk mass in dust against the estimated mass of the central star (dust mass obtained with q-values of 2.5 and 3) and mass accretion rate (dust mass with $q = 3$ and stellar ages smaller and greater than 2 Myr) respectively. In the $0.3-2$ $M_\odot$ range in stellar mass the dust mass does not show any trend (for $q = 2.5$: $3 \times 10^{-5} < M_{dust} < 2 \times 10^{-4}$ $M_\odot$; for $q = 2.5$: $4 \times 10^{-5} < M_{dust} < 2 \times 10^{-3}$ $M_\odot$). The two YSOs with $M_\star \lesssim 0.3$ $M_\odot$ have lower dust masses than all the other YSOs for both $q = 2.5$ and 3. However, the range in stellar mass spanned by our sample is rather limited and particularly biased toward YSOs with late-K and early-M spectral types. From the upper limits obtained at 1.3 mm by Schaefer et al. (2009) for 14 T-Tauri stars with spectral types later than $\approx$M2 ($F_{1.3\ mm} \lesssim 5-20$ mJy) and from the detection of very low disk masses around substellar objects in Taurus-Auriga (Klein et al. 2003, Scholz et al. 2006), it is likely that a correlation between the disk mass in dust and the mass of the central star exists. High sensitivity millimeter observations are needed to constrain the disk masses in dust around very low mass PMS stars. In Fig. 10 a trend of higher mass accretion rates for the more massive disks in dust may be

present in the data, but the scatter is still very significant (a similar result is obtained for the case of $q = 2.5$). Other relations between the dust properties (β, dust mass) and the stellar ones (e.g. stellar luminosity, effective temperature) have been investigated, but no significant correlations were found.

Finally, we have compared the values of β obtained in this paper with those derived in Natta et al. (2004) for a sample of six intermediate mass Herbig Ae stars and three lower mass T Tauri stars. From the two-sided Kolmogorov-Smirnov test, the probability that the β values from the two samples come from the same distribution is about 88%, indicating that the disks in the two samples have similar dust properties in terms of grain growth (in the Natta et al. 2004 sample only one object, the Herbig Ae star HD150193, has a relatively high $\beta = 1.6 \pm 0.2$, compatible with non-evolved ISM-like dust grains).

5. Summary

We have analysed the sub-mm/mm SED out to 3 mm of a sample of 21 class II T-Tauri stars in the Taurus-Auriga star forming region. This sample comprises about the 60% of the "isolated" class II YSOs with an estimated stellar mass greater than
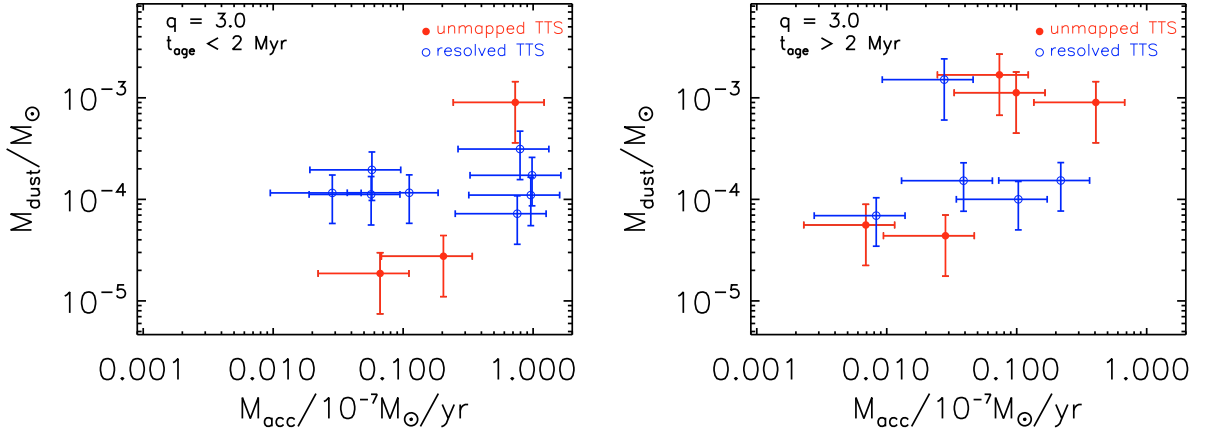
Fig. 10. Disk mass in dust plotted against the mass accretion rate for the sources in our sample. In the left and right panels we included the objects with estimated ages of less and more than 2 Myr respectively. The dust mass has been obtained adopting a value of 3 for the power index q of the dust grain size distribution. The stellar mass accretion rate has been estimated following the method described in Sect. 2.4. Open blue points represent the spatially resolved disks, whereas the filled red points are for the unmapped ones. The errorbars in the mass accretion rate take into account the typical intrinsic time-variability of the accretion rates. The errorbars in the dust mass estimates do not include our uncertainty on the actual value of q.

$\approx 0.4\ M_\odot$. It also comprises approximately 1/3 of the isolated class II wich have been observed at 0.85 mm to have a flux less than 100 mJy, for which we provide the first 3 mm detections thanks to sensitive PdBI observations. Our main findings are summarized below:

1. For all the sources in our sample the millimeter opacity spectral index β is significantly lower than the value obtained for the dust in the ISM. For the 13 spatially resolved disks this is a clear evidence of the presence in the outer disk regions of dust grains as large as at least 1 mm. For the eight unmapped sources, assuming disk outer radii comparable to the resolved sources, low β values are found as well, which suggests that even for these fainter sources 1 mm-sized grains are in the disk outer regions. This confirms over a larger sample and less massive disks the results obtained by past observations on T-Tauri stars (e.g. Rodmann et al. 2006 and references therein).

2. No significant evidence of an evolutionary trend for the millimeter opacity spectral index β has been found. This indicates that the dust grain growth to ~1 mm-sizes is a very fast process in a protoplanetary disk, which appears to occur before a YSO enters into the class II evolutionary stage. Also, the amount of these large grains in the disk outer regions does not appear to decline throughout all the class II evolutionary stage.

3. Only for nine sources in our sample a power law index for the grain size distribution of the ISM, $q_{ISM} \approx 3.5$, is consistent with the sub/mm-mm SED. Instead, most of the disks show evidence of a smaller q-value.

4. We have not found any significant correlation between the dust properties, namely grain growth and dust mass in the disk outer regions, and the properties of the central star, including the mass accretion rate onto the stellar surface. However, our sample contains mostly YSOs with a narrow range in spectral types, namely between late-K and early-M, and it is possible that a correlation between the disk mass in dust and the stellar mass will become apparent if one also considers disks around late-M spectral types.

5. The six faintest sources in our sample with $F_{1\ mm} < 50$ mJy show a spectral index between 1 and 3 mm that is on average lower than the spectral index of the brighter sources.

This may indicate either that for these fainter, yet unmapped disks the emission from the optically thick inner disk is much more significant than for the brighter sources or that the dust grains in the outer regions of these fainter disks are even larger than in the brighter YSOs, possibly up to 10 cm if $q = 3$. The latter hypothesis would imply on average a lower absolute value for the millimeter opacity coefficient for these fainter disks. Taking into account this effect through a physical model for the dust properties, we found in the case of a value for the power index of the grain size distribution $q = 3$ an anticorrelation between β and the disk dust mass, which would indicate that larger dust grains are found in the outer parts of the more massive disks (in dust).

In the future, with the advent of the next sub-mm/mm facilities (both new interferometers like ALMA and technical improvements in the existing arrays, like for example the E-VLA), it will be possible to extend the investigation of the dust properties to fainter circumstellar disks around the lowest mass PMS stars and brown dwarfs. Furthermore, thanks to the considerable enhancements in both high angular resolution and sensitivity, which these facilities will provide, it will be possible to determine their spatial extension.

References

Adachi, I., Hayashi, C., & Nakazawa, K. 1976, Prog. Theor. Phys., 56, 1756
Adams, F. C., Emerson, J. P., & Fuller, G. A. 1990, ApJ, 357, 606
Altenhoff, W. J., Thum, C., & Wendker, H. J. 1994, A&A, 281, 161
Andrews, S. M., & Williams, J. P. 2005, ApJ, 631, 1134
Andrews, S. M., & Williams, J. P. 2007, ApJ, 659, 705
Andrews, S. M., Wilner, D. J., Hughes, A. M., Qi, C., & Dullemond, C. P. 2009, ApJ, 700, 1502
Baraffe, I., Chabrier, G., Allard, F., et al. 1998, A&A, 337, 403
Barge, P., & Sommeria, J. 1995, A&A, 295, L1
Beckwith, S. V. W., & Sargent, A. I. 1991, ApJ, 381, 250
Beckwith, S. V. W., Sargent, A. I., Chini, R. S., et al. 1990, AJ, 99, 924
Bertout, C., Robichon, N., & Arenou, F. 1999, A&A, 352, 574
Bessell, M. S., & Brett, J. M. 1988, PASP, 100, 1134
Brauer, F., Dullemond, C. P., Johansen, A., et al. 2007, A&A, 469, 1169

Bouwman, J., Meeus, G., de Koter, A., et al. 2001, A&A, 375, 950
Briceño, C., Hartmann, L., Stauffer, J. R., et al. 1998, AJ, 115, 2074
Briceño, C., Luhman, K. L., Hartmann L., Stauffer, J. R., & Kirkpatrick, J. D. 2002, ApJ, 580, 317
Calvet, N., & Gullbring, E. 1998, ApJ, 509, 802
Calvet, N., D'Alessio, P., Hartmann, L., et al. 2002, ApJ, 568, 1008
Calvet, N., Muzerolle, J., Briceño, C., et al. 2004, AJ, 128, 1294
Carpenter, J. M. 2001, AJ, 121, 2851
Chiang, E. I., & Goldreich, P. 1997, ApJ, 490, 368
Cutri, R. M., et al. 2003, 2MASS All Sky Catalog of point sources
Davies, D. R., & Ryan, E. V. 1990, Icarus, 83, 156
Draine, B. T. 2006, ApJ, 636, 1114
Draine, B. T., & Lee, H.-M. 1984, ApJ, 285, 89
Dullemond, C. P., Dominik, C., & Natta, A. 2001, ApJ, 560, 957
Dutrey, A., Guilloteau, S., Duvert, G., et al. 1996, A&A, 309, 493
Gullbring, E., Calvet, N., Muzerolle, J., et al. 2000, ApJ, 544, 927
Gullbring, E., Hartmann, L., Briceño, C. 1998, ApJ, 492, 323
Hartigan, P., & Kenyon, S. J. 2003, ApJ, 583, 334
Hartmann, L. 2001, AJ, 121, 1030
Herczeg, C. J., & Hillenbrand, L. A. 2008, ApJ, 681, 594
Hughes, M. A., Wilner, D. J., Qi, C., et al. 2008, ApJ, 678, 1119
Isella, A., Carpenter, J. M., & Sargent, A. F. 2009, ApJ, 701, 260
Itoh, Y., Hayashi, M., Tamura, M., et al. 2005, ApJ, 620, 984
Jensen, E. L. N., Koerner, D. W., & Mathieu, R. D. 1996, AJ, 111, 2431
Jensen, E. L. N., Dhital, S., Stassun, K. G., et al. 2007, AJ, 134, 241
Kenyon, S. J., & Hartmann, L. 1995, ApJS, 101, 117
Kessler-Silacci, J., Augereau, J. C., Dullemond, C. P., Geers, V., Lahuis, F., et al. 2006, ApJ, 639, 275
Kitamura, Y., Momose, M., Yokogawa, S., et al. 2002, ApJ, 581, 357
Klahr, H. H., & Henning, T. 1997, Icarus, 128, 213
Klein, R., Apai, D., Pascucci, I., Henning, Th., & Waters, L. B. F. M. 2003, ApJ, 593, 57
Koerner, D. W., Chandler, C. J., & Sargent, A. I. 1995, ApJ, 452, 69
Kwon, W., Looney, L. W., Mundy, L. G., Chiang, H., & Kemball, A. 2009, ApJ, 696, 841
Leggett, S. K. 1992, ApJS, 82, 351
Leinert, C., Zinnecker, H., Weitzel, N., et al. 1993, A&A, 278, 129
Lommen, D., Wright, C. M., Maddison, S. T., et al. 2007, A&A, 462, 211
Lommen, D., Maddison, S. T., Wright, C. M., 2009, A&A, 495, 869
Luhman, K. L. 1999, ApJ, 525, 466
Malfait, K., Waelkens, C., Waters, L. B. F. M., et al. 1998, A&A, 332, 25

Mannings, V., & Emerson, J. P. 1994, MNRAS, 267, 361
Mathieu, R. D. 1994, ARA&A, 32, 465
Mathis, J. S., Rumpl, W., & Nordsieck, K. H. 1977, ApJ, 217, 425
Meyer, M. R., Calvet, N., & Hillenbrand, L. A. 1997, AJ 114, 288
Miyake, K., & Nakagawa, Y. 1993, Icarus, 106, 20
Mundy, L. G., Looney, L. W., Erickson, W., et al. 1996, ApJ, 464, L169
Natta, A., Testi, L., Neri, R., Shepherd, D. S., & Wilner, D. J. 2004, A&A, 416, 179
Ohashi, N., Hayashi, M., Kawabe, R., et al. 1996, ApJ, 466, 317
Padgett, D. L., Brandner, W., Stapelfeldt, K. R., et al. 1999, AJ, 117, 1490
Palla, F., & Stahler, S. W. 1999, ApJ, 525, 772
Pinte, C., Fouchet, L., Ménard, F., Gonzalez, J.-F., & Duchêne, G. 2007, A&A, 469, 963
Pollack, J. B., Hollenbach, D., Beckwith, S. 1994, ApJ, 421, 615
Pollack, J. B., Hubickyj, O., Bodenheimer, P., et al. 1996, Icarus, 124, 62
Hollenbach, D., Beckwith, S., Simonelli, D. P., Roush, T., & Fong, W. 1994, ApJ, 421, 615
Reipurth, B., & Zinnecker, H. 1993, A&A, 278, 81
Rieke, G. H., & Lebofsky, M. J. 1985, ApJ, 288, 618
Rodmann, J., Henning, T., Chandler, C. J., Mundy, L. G., & Wilner, D. J. 2006, A&A, 446, 211
Safronov, V. S., & Zvjagina, E. V. 1969, Icarus, 10, 109
Schaefer, G. H., Dutrey, A., Guilloteau, S., Simon, M., & White, R. J. 2009, ApJ, 710, 698
Schmidt-Kaler, T. 1982, in Landolt-BornsteinGroup VI, 2, ed. K.-H. Hellwege (Berlin: Springer), 454
Scholz, A., Jayawardhana, R., & Wood, K. 2006, ApJ, 645, 1498
Simon, M., & Prato, L. 1995, ApJ, 450, 824
Simon, M., Chen, W.-P., Howell, R. R., Benson, J. A., & Slowick, D. 1992, ApJ, 384, 212
Takeuchi, T., & Lin, D. N. C. 2005, ApJ, 623, 482
Tanaka, H., Himeno, Y., & Ida, S. 2005, ApJ, 625, 414
Testi, L., Natta, A., Shepherd, D. S., & Wilner, D. J. 2001, ApJ, 554, 1087
Testi, L., Natta, A., Shepherd, D. S., et al. 2003, A&A, 403, 323
Throop, H. B., Bally, J., Esposito, L. W., et al. 2001, Science, 292, 1686
Valenti, J. A., Basri, G., & Johns, C. M. 1993, AJ, 106, 2024
Warren, S. G. 1984, ApOpt 23, 1206
Weidenschilling, S. J. 1977, MNRAS, 180, 57
Weingartner, J. C., & Draine, B. T. 2001, ApJ, 548, 296
Wilner, D. J., Ho, P. T. P., Kastner, J. H., et al. 2000, ApJ, 534, L101
Zubko, V. G., Mennella, V., Colangeli, L., et al. 1996, MNRAS, 282, 1321